Multiphysics Simulation of a Self-heating Paraffin Membrane Microactuator

Panos Lazarou and Christine Rotinat*
CEA LIST, Interactive Robotics Laboratory, France
*Corresponding author: CEA Saclay - DIGITEO Moulon, DRT/LIST/DIASI/LRI, Point courrier n°178, F-91191Gif-sur-Yvette Cedex, France, christine.rotinat-libersa@cea.fr

Abstract: A grand variety of microactuator technologies and demonstrators has been introduced during the last years. Of particular interest are the microactuators based on phase change materials and especially paraffin wax, which can volumetrically expand up to 15%, providing high force actuation. The object of this study is the numerical validation of a paraffin microactuator concept by coupling multiple physics and phase change. The coupling procedure is explained, along with the approximations for the various material properties and the phase change equations. Finally, the results of the simulations and the available experimental data are compared and discussed, showing that this kind of multiphysics coupling and simulation approximates successfully the complex real phenomena.

Keywords: multiphysics, joule heating, phase change, fluid-structure interaction

1. Introduction

Over the past decade many low voltage electromechanical implementations based on various actuation principles have been presented, such as electrostatic [1,2,3], piezoelectric [4,5], magnetic [6,7], thermal [8,9] and phase change. The last category includes shape-memory actuators utilizing solid-to-solid transition [10,11] and solid-to-liquid phase change materials like e.g. polyethyelene and paraffin, where the phase transition incurs a change in geometry, thus providing the required force and movement.

Paraffin wax is especially preferred in many applications due to its unique property of volumetrically expanding up to 10-15% during heating and phase change. The main advantages of this type of systems are the large stroke and high force capabilities [12,13,14,15], as well as the variety of the manufacturing techniques available. Paraffin wax can significantly expand even with loads of hundreds of MPa.

This paper presents a numerical simulation of the actuator concept introduced in [15] (Figure 1) through the coupling of multiple physics: Joule heating, heat transfer, thermal dilatation and solid to liquid phase change of the paraffin, as well as fluid-structure interaction with the membrane. The material properties, the phase change equations, the approximations in setting up the model and the coupling procedure are discussed. The membrane deflection as a function of the temperature is finally calculated and compared to the experimental results, showing similar behavior.

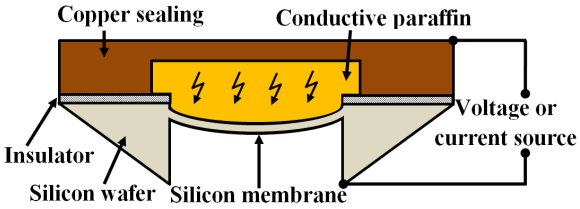

Figure 1. Paraffin self-heating phase change microactuator, adapted and simplified from [15].

2. The actuation concept

The actuator shown in Figure 1 consists of a chamber filled with a composite of paraffin wax and conductive carbon black particles, a copper sealing chip and a doped n+ silicon membrane. The application of a voltage or current between the copper sealing and the silicon membrane/wafer results in the Joule heating of the paraffin domain. As the composite's temperature increases, it expands -eventually changing phase into liquid state- and deflects the thin membrane, thus providing the necessary force and movement of the actuator. Once all the paraffin inside the chamber has melted, the membrane reaches its maximum deflection.

According to [15], the actuator dimensions are 10x10 mm with a 6x6 mm, 45 μm thick silicon membrane. The authors also used two kinds of paraffin waxes, a refined paraffin with a melting point of 42-44 °C (we assumed it to be n-docosane $C_{22}H_{46}$ because of the same melting point) and n-tetracosane $C_{24}H_{50}$ with two phase transitions at 48 °C and 50.1 °C. Each paraffin is mixed with carbon black at a 2%-4% volume

fraction. The reported paraffin initial volume is 5.1 μl and 2.1 μl for n-docosane and n-tetracosane respectively. These values have been used to estimate the approximate dimensions of the paraffin chamber. Table 1 summarises all the known information given in [15] regarding the actuator geometry and paraffin properties.

3. Problem specifications and boundary conditions

3.1 Geometry, materials and properties

To perform the study, a 2D geometry has been chosen, representing a slice across the center of the actuator. Due to symmetry, only half of the actuator's geometry is actually modeled, as seen in Figure 2, with an assumed out-of-plane depth of 6mm. The overall length is set to 5 mm and the length and thickness of the membrane to 3 mm and 45 μm respectively.

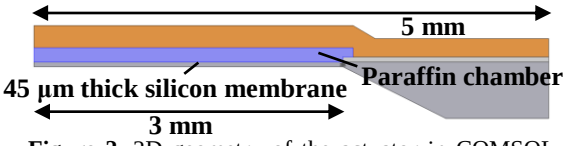

Figure 2. 2D geometry of the actuator in COMSOL with an assumed out-of-plane thickness of 6mm.

3.2 Basic material properties (classic materials)

The materials -excluding the paraffin wax- used for the simulation include copper, n-silicon and Si_3N_4. Their properties are imported directly from COMSOL's material library.

3.3 Basic paraffin wax material properties

Due to the lack of sufficient information in [15], several assumptions, approximations and usage of data from literature were necessary to properly define the thermophysical and electrical properties of the two paraffin waxes so as to construct a multiphysics model in COMSOL. These are collectively presented in Table 1. Some of them are approximate (marked with *), as explicit ones for some physical parameters could not be found. Additionally, there were often values that differed either slightly or significantly –depending on the reference, especially for the density and the specific heat capacity. The values that seemed to agree the most (within a small deviation range, with the findings of most articles and online data sources) are used.

The symbol C_p represents the specific heat capacity under constant pressure, ρ the density, ε_r the relative electric permittivity, σ the electric conductivity, k the thermal conductivity, P_r the Prandtl number, T the temperature, ΔH the latent heat during the phase change and μ the dynamic viscosity. Additionally, the indices s, l and m in the above mentioned quantities imply the solid phase (solid 1 and 2 phases for $C_{24}H_{50}$), liquid phase and melting temperatures respectively.

Table 1: Properties of paraffins used in the model

Property	**$C_{22}H_{46}$ paraffin**	**$C_{24}H_{50}$ paraffin**
P_r	40 [16]	
k ($W \cdot m^{-1} \cdot K^{-1}$)	≈0.21 [17]	
ε_r	2.5 [18]	
σ ($S \cdot cm^{-1}$)	σ(T)	
$C_{p,s}$ ($kJ \cdot kg^{-1} \cdot K^{-1}$)	2.48[17]	1.97[17]
$C_{p,l}$ ($kJ \cdot kg^{-1} \cdot K^{-1}$)	2.76[17]	2.10[17]
ρ_s ($kg \cdot m^{-3}$)	829 [17]	866 [17]
ρ_l ($kg \cdot m^{-3}$)	755*	774 [17]
ΔH ($kJ \cdot kg^{-1}$)	252 [19]	92.42 and 162 [19]
T_s (°C) *	41	46.2 and 47.8
T_l (°C) *	44.5	50.6
T_m (°C) *	42.75	47 and 50.1
dT (°C) *	1.75	0.8 and 0.47
μ (Pa·s)	μ(T) (discussed in 4.2.2)	

The experimental results of [15] show that the phase transition takes place in a small region centered on the melting temperature T_m. Let that region be equal to 2*dT (where dT is the half width); the temperatures of solid and liquid phase are then deduced.

Also, due to the fact that the electric resistivity and conductivity in paraffins are highly non-linear, a step distribution profile of the resistivity near the melting temperature was assumed, similar to the data found in [20] for a composite of paraffin wax with carbon nanotubes. The values of resistivity range from 0.053 kΩ·cm for temperatures below T_m up to 1 kΩ·cm for temperatures above T_m. Figure 3 shows the profile of the electric conductivity

versus temperature that is used in the simulations.

Additionally, from the results presented in [17], the thermal conductivity of the paraffin shows no significant variations with temperature, therefore it is assumed that k(T) is constant.

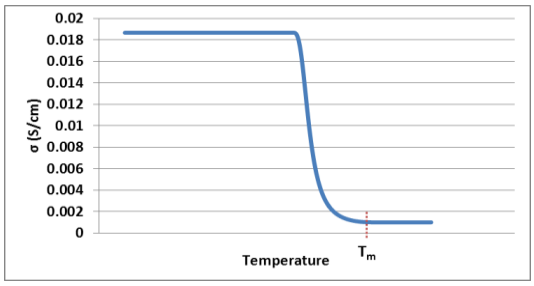

Figure 3. Plot of the electric conductivity σ with temperature.

3.4 Loading and boundary conditions

The initial conditions and the settings for the various physics interfaces used are given below. For the electric currents interface a potential difference is used. The bottom outer boundaries of the silicone are set to ground, while the top outer boundaries of the copper domain being set to a potential V_{app}=3.25 V for $C_{22}H_{46}$ and V_{app}=5.3 V for $C_{24}H_{50}$. Thus, approximately 1.9 W is dissipated, as reported in [15]. Due to the transient nature of the problem, the voltage is applied as a smoothed step function with a zero value for t=0 s and reaching the maximum value V_{app} after 0.1 s.

For the thermal analysis of the system, the governing equations of heat transfer in liquids and solids are used. All domains are set to an initial temperature T_{init}=20 °C and all the outer boundaries of the geometry are submitted to an air convection condition with a convection coefficient of 5 $W \cdot m^{-2} \cdot K^{-1}$. In order to couple the Joule heating from the application of the potential difference of the electric currents interface to the heat transfer interface, the power dissipation density is used as a domain heat source.

The following volume force is set to act on the paraffin domain in order to represent the gravity effect:

$$F_v = -\rho_{app} * g \quad (1)$$

3.5 Solving

In order to account for the time dependency of the problem, as well as for the non-linear behavior of the phase change in the paraffin wax, transient analysis was used. A very dense mesh was required in the paraffin domain in order to achieve convergence during phase changes. It consists of around 15.000 domain elements and 74500 degrees of freedom, while the time stepping of the BDF time-dependent solver was explicitly set to 5 ms.

4. Multiphysics coupling specifications

4.1 Multiphysics problem

In order to simulate the transient actuation problem where multiple physics have to be combined, a coupling of three different COMSOL physics was required. We therefore used the electric currents, the heat transfer and the fluid-structure interfaces. A simplified representation of the way they interact with each other is shown in Figure 4, where P, u_{fluid} and u_{solid} stand for fluid pressure and velocity field respectively.

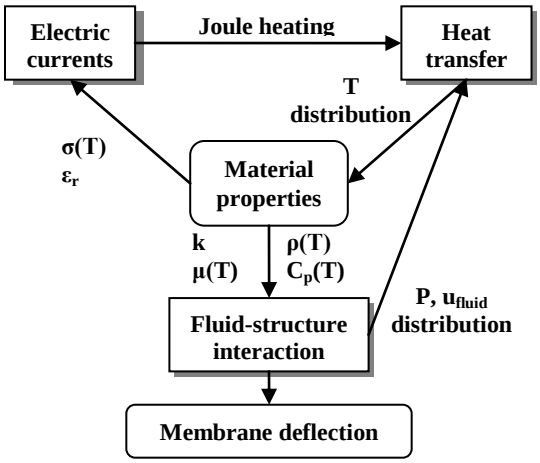

Figure 4. Simplified coupling diagram and operational loop of the various physics used.

The electric currents interface applies a voltage or current between the two contact boundaries of the actuator (shown in Figure 1). The resulting current passing through the paraffin domain produces Joule heat due to the paraffin's resistivity. This thermal power dissipation is used as a heat input source to the

heat transfer module and thus the overall temperature distribution for all the domains is calculated. As a consequence, it defines the momentary values of the paraffin's following temperature dependent quantities ρ, C_p, μ and σ.

Then, the electric currents and the fluid-structure interaction interfaces receive these variables as inputs so as to calculate the passing current inside the paraffin domain and the fluid pressure-velocity distributions and membrane deflection respectively. The velocity and pressure distributions are also used as inputs in the heat transfer interface.

4.2 Phase change specific physical properties

4.2.1 Pure paraffin wax properties

The phase change of the paraffin waxes is effectuated with the usage of user-defined functions in the material properties. The COMSOL documentation describes this procedure of modeling for phase change materials. Let a be the fraction of the fully liquid phase. The transition from solid to liquid can be defined with the innate COMSOL equation flc2hs (Heaviside function) that smoothly varies the values of a from 0, representing full absence of liquid phase, to 1, representing fully liquid phase. Obviously the solid fraction is the quantity $(1-a)$. The apparent heat capacity C_{p_app} is therefore given by the formula:

$$C_{p,app} = C_{p,s}*(1-\alpha)+C_{p,l}*\alpha + \Delta H*D \quad (2)$$

where D is a Gaussian Dirac pulse defining the distribution of the latent heat ΔH in the transition area. Its formula is given by:

$$D=\frac{e^{\frac{-(T-T_m)^2}{dT^2}}}{\sqrt{\pi dT}} \quad (3)$$

The equation for the density of the wax is:

$$\rho_{app}=\frac{\rho_s*C_{p,s}*(1-\alpha)+\rho_l*C_{p,l}*\alpha}{C_{p,s}*(1-\alpha)+C_{p,l}*\alpha} \quad (4)$$

Equations (2) and (4) are in fact temperature dependent and define the transition between the solid and the liquid phase both thermally (through the change in thermal conductivity and specific heat capacity) and mechanically (through the change in density that produces a volume expansion); the thermal conductivity is assumed to be constant, as mentioned. In the case of $C_{24}H_{50}$ with two phase transitions the above formulas are similar but more complex with the inclusion of two fraction variables a_1 for the solid 1-to-solid 2 and a_2 for the solid 2-to-liquid phase change.

4.2.2 Composite wax (paraffin-carbon) properties

The actual material used in [15] is a composite of paraffin with carbon black particles (ρ_{car}=2260 kg·m^{-3}, $C_{p,car}$=695 J·kg^{-1}·K^{-1} and k_{car}=23.82 W·m^{-1}·K^{-1}), therefore the presence of the carbon concentration has to be taken into account. Using the mixture rule and a volumetric fraction of f_v=2% carbon black, the overall density and specific heat capacity of the composite can be calculated by [20]:

$$\rho=\rho_{app}*(1-f_v)+\rho_{car}*f_v \quad (5)$$

$$C_p=\frac{\rho_{app}*C_{p,app}*(1-f_v)+\rho_{car}*C_{p,car}*f_v}{\rho} \quad (6)$$

Equations (5) and (6) define the material properties of the composite paraffin waxes. The wax phase change effects are included in the terms ρ_{app} and C_{p_app}. Figures 5 and 6 present the distribution of the overall specific heat capacity and density of the two composite waxes (2% vol. carbon black) with temperature; the composite's thermal conductivity is calculated to be constant with a value of k≈0.3 W·m^{-1}·K^{-1} [21].

To represent the volumetric expansion during the phase transition, the composite paraffins are modeled as a highly viscous liquids with high density and viscosity below the melting temperature and lower density and viscosity above the melting temperature. As already mentioned, the coupling of the fluid-structure interaction interface with the rest of the physics is performed through the values of the temperature dependent quantities ρ, C_p and μ, which act as inputs.

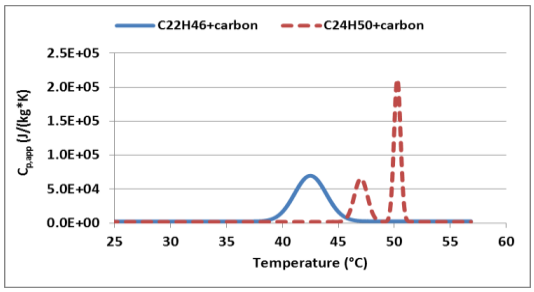

Figure 5. Plot of specific heat capacity versus temperature for the two paraffin composites.

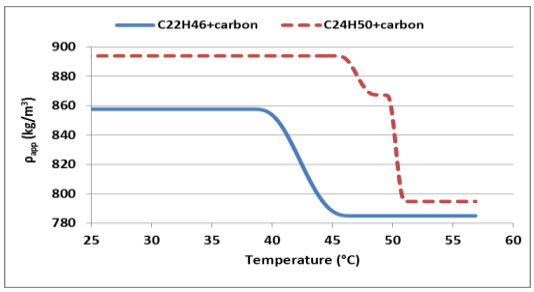

Figure 6. Plot of density versus temperature for the two paraffin composites.

Thus the two paraffin composites are considered as liquids of variable viscosity, defined with smoothed step functions, as seen in Figure 7. This effectively represents a smoothed ramp function ranging from a very high value for temperatures below T_m (solid phase) and a small value calculated using the definition of the Prandtl number for temperatures above T_m (liquid phase):

$$\mu = \frac{P_r k}{C_p} \qquad (7)$$

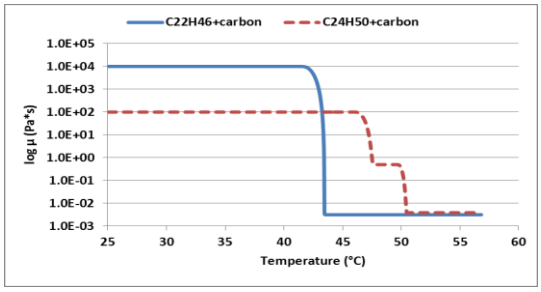

Figure 7. Plot of the log of viscosity versus temperature for the two paraffin composites.

As C_p is the specific heat capacity of the composite, the effect of carbon is also taken into account. For the composite of $C_{22}H_{46}$ the values of 10^4 Pa·s for the solid phase and the computed value of 3.3 mPa·s for the liquid phase are used. For the $C_{24}H_{50}$ the values 10^2 Pa·s (for numerical convergence reasons), 0.5 Pa·s (an intermediate value to represent a mushy, gel-like zone) and 3.8 mPa·s were selected.

5. Validation of the model

In this section the results of the simulations are presented for the two cases of paraffin waxes and are compared to the experimental measurements from [15]. First of all, for the $C_{22}H_{46}$ wax, Figure 8 shows a comparison of the calculated and measured deflections of the silicon membrane versus the temperature at the outer surface of the copper chip.

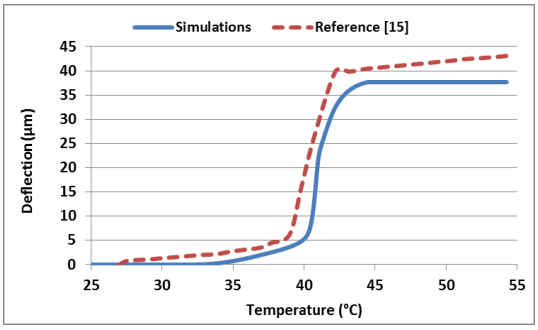

Figure 8. Plot of simulated membrane deflection versus external copper chip temperature for the composite wax $C_{22}H_{46}$, comparison with [15].

It can be observed that the simulation results are relatively close to the experimental ones. Before the phase change takes place, there is a linear increase in the experimental deflection; similarly for the purely liquid phase. This linear behavior is not represented by our model since we assumed constant values of ρ and μ in the pure solid and liquid phases. An improvement of the model could be to take into account the fact that the density of the solid paraffin decreases linearly with the increase of temperature.

At the end of the phase change (at fully liquid phase) a deflection difference of approximately 3.3 μm (40 μm versus calculated 37.7 μm) can be attributed to the deflection during the solid linear dilatation regime, the approximations as well as the transition modeling we have used. While the phase transition at the experimental results actually starts at around 38 °C (external copper chip temperature), in the simulations it begins a little

earlier, around 34 °C. This can be attributed to the air convection coefficient used in our model and again in the lack of sufficient data from [15].

Figure 9 shows a time step of the transition phase, where the deflection and stress of the membrane, the liquid fraction *a* and the temperature distribution in the composite wax can be seen. The fully white area in the paraffin domain represents the fully liquid phase, the various shades of yellow the intermediate phase (mushy zone) and the darker red colour to the right the almost solid phase (very low current density due to the existence of the dielectric). The deflection at the center of the membrane at this time step is 28.9 µm.

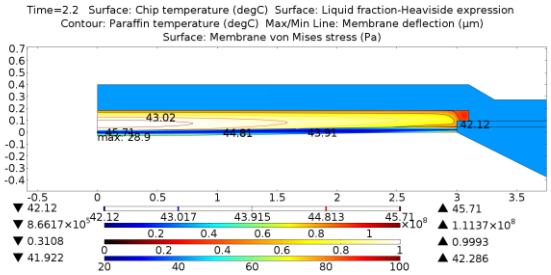

Figure 9. Plot of liquid fraction, temperature distribution and membrane deflection and stress for t=2.2 s.

The simulation results for the membrane deflection of the actuator containing the composite $C_{24}H_{50}$ are shown in Figure 10.

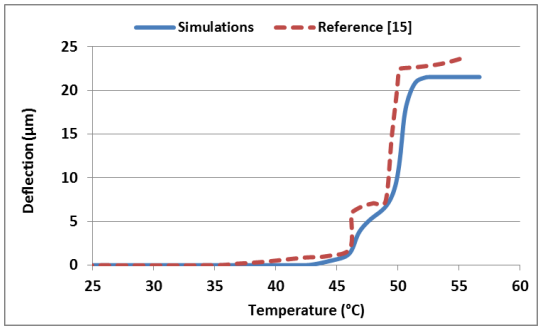

Figure 10. Plot of membrane deflection versus external copper chip temperature for $C_{24}H_{50}$, comparison with reference [14].

Similarly, there is a difference of approximately 1 µm (22.54 µm versus calculated 21.5 µm) as well as a linear behaviour that is not represented by the modeling of the transitions. A relatively good accordance of the reference and the simulation data can be otherwise observed.

Figure 11 shows the maximum deflection achieved (21.5 µm) when the whole paraffin domain is in liquid phase with a dynamic viscosity of 3.88 mPa·s.

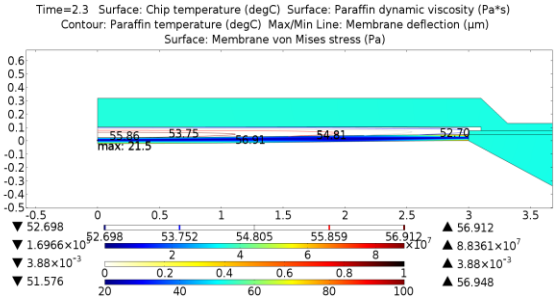

Figure 11. Plot of temperature distribution, viscosity, membrane deflection and stress and for t=2.3 s.

6. Conclusions

A numerical simulation of the operation of a paraffin phase change microactuator is presented in this paper, along with the coupling of the simultaneous physics of phase change, heat propagation, Joule heating and fluid structure interaction. Several approximations and assumptions had to be made in order to create a model as close as possible to the real behavior of the composite wax actuator. Additional sources of inaccuracy for the results are the simplified geometry, the border effects (2D slice model, 6mm out-of-plane depth which equals wax depth only) and the absence of sufficient information about the type of air convection (natural or forced).

Generally, the results are in a relatively good accordance with the experimental data; the calculated deflection of the actuator's membrane closely follows the real one. Knowledge of all the properties of the specific paraffins and the experimental conditions would obviously provide more accurate results. Nevertheless, the coupling of multiple different physics was successful and thus this kind of complex simulations can be definitely used as a prediction and optimization tool for real experiments.

7. References

1. Ching-Chen Tu, Kuohao Fanchiang, Cheng-Hsien Liu, "Rotary electrostatic micromirror switches using wafer-scale processing and assembly", *Microsystem Technologies*, 12(12), 1099-1108 (2006)

2. Mustafa Emre Karagozler, Seth Copen Goldstein and J. Robert Reid, "Stress-Driven MEMS Assembly + Electrostatic Forces = 1mm Diameter Robot", *In Proceedings of the IEEE International Conference on Intelligent Robots and Systems (IROS '09)*, 2763-2769 (2009)
3. A. Grira, B. Legrand, C. Rotinat-Libersa, E. Mairiaux and L. Buchaillot, "Optimal design of non-intuitive compliant microgripper with high resolution", *IEEE/RSJ International Conference on Intelligent Robots and Systems, IROS2011*, 45-50 (2011)
4. R. Maeda, J.J. Tsaur, S.H. Lee, M. Ichiki, "Piezoelectric microactuator devices", *J. Electroceramics*, 12 (1/2), 89–00 (2004)
5. T. Mashimo and S. Toyama, "Rotary-linear piezoelectric microactuator with a cubic stator of side length 3.5 mm", *IEEE Trans Ultrason Ferroelectr Freq Control*, 57(8), 1825-1830 (2010)
6. Karl Vollmers, Dominic R. Frutiger, Bradley E. Kratochvil and Bradley J. Nelson, "Wireless resonant magnetic microactuator for untethered mobile microrobots", *Appl. Phys. Lett.*, 92 (14), 144103 (2008)
7. K. Kobayashi and K. Ikuta, "3D Magnetic Microactuator Made of Newly Developed Magnetically Modified Photocurable Polymer and Application to Swimming Micromachine and Microscrewpump", *Micro Electro Mechanical Systems, MEMS 2009. IEEE 22nd International Conference on*, 11-14 (2009)
8. R. Cragun and L. Howell, "Linear thermomechanical microactuators", *Proc. ASME IMECE*, 181-188 (1999)
9. Gih-Keong Lau, J.F.L. Goosen, F. van Keulen, Chu Duc Trinh; P.M. Sarro, "Polymeric Thermal Microactuator With Embedded Silicon Skeleton: Part I—Design and Analysis", Journal of Microelectromechanical Systems, 17(4), 809 –822 (2008)
10. Y. Bellouard, "Shape memory alloys for microsystems: A review from a material research perspective," *Mater. Sci. Eng. A*, 481/482, 582–589 (2008)
11. Kai Liu, Chun Cheng, Zhenting Cheng, Kevin Wang, Ramamoorthy Ramesh and Junqiao Wu, "Giant-Amplitude, High-Work Density Microactuators with Phase Transition Activated Nanolayer Bimorphs", Nano Lett., 12 (12), 6302–6308 (2012)
12. E. T. Carlen and C. H. Mastrangelo, "Electrothermally activated paraffin microactuators," *J. Microelectromech. Syst*., 11(3), 165–174 (2002)
13. L. Klintberg et al, "A large stroke, high force paraffin phase transition actuator", *Sensors and Actuators A: Physical*, 96 (2–3), 189-195 (2002)
14. H.J. Sant et al, "An in situ heater for a phase-change-material-based actuation system", J. Micromech. Microeng. 20, 085039 (2010)
15. F. Goldschmidtboing et al., "A novel self-heating paraffin membrane micro-actuator", *Micro Electro Mechanical Systems 2008, MEMS 2008. IEEE 21st International Conference on*, 531-534 (2008)
16. E-H Hirschel, "*Numerical Flow Simulation II: Cnrs-dfg Collaborative Research Programme, Results 1998-2000",* 121-122, Springer-Verlag Berlin and Heidelberg GmbH & Co. K (2001)
17. N. Ukrainczyk et al, "Thermophysical Comparison of Five Commercial Paraffin Waxes as Latent Heat Storage Materials", *Chemical and Biochemical Engineering Quarterly Journal*, 24, 129-137 (2010)
18. The Engineering Toolbox website, http://www.engineeringtoolbox.com
19. National Institute of Standards and Technology Chemistry Book, http://webbook.nist.gov/chemistry/
20. K. Zhang, B. Han and X. Yu, "Electrically conductive carbon nanofiber/paraffin wax composites for electric thermal storage", *Energy Conversion and Management*, 64, 62-67 (2012)
21. A. V. Arasu et al., "Thermal performance enhancement of paraffix wax with AL2O3 and CuO nanoparticles – a numerical study", *Frontiers in Heat and Mass Transfer (FHMT*), 2, 043005 (2011)

8. Acknowledgements

The authors are very grateful to the French Ministry of economy, industry and employment (Direction Générale de la Compétitivité, de l'Industrie et des Services - DGCIS) for their financial support under the grant 102930231 (Mediate, ITEA2 labeled project, EUREKA cluster program).